EBioMedicine 34 (2018) 189–200

Contents lists available at ScienceDirect

EBioMedicine

journal homepage: www.ebiomedicine.com

EBioMedicine
Published by THE LANCET

Research Paper

The Autism-Related Protein PX-RICS Mediates GABAergic Synaptic Plasticity in Hippocampal Neurons and Emotional Learning in Mice

Tsutomu Nakamura *, Fumika Sakaue, Yukiko Nasu-Nishimura, Yasuko Takeda, Ken Matsuura, Tetsu Akiyama

Laboratory of Molecular and Genetic Information, Institute for Quantitative Biosciences, The University of Tokyo, 1-1-1, Yayoi, Bunkyo-ku, Tokyo 113-0032, Japan.

ARTICLE INFO

Article history:
Received 6 March 2017
Received in revised form 4 July 2018
Accepted 11 July 2018
Available online 22 July 2018

Keywords:
Autism
Inhibitory synaptic plasticity
Emotion
$GABA_A$ receptor
Trafficking
Amygdala

ABSTRACT

GABAergic dysfunction underlies many neurodevelopmental and psychiatric disorders. GABAergic synapses exhibit several forms of plasticity at both pre- and postsynaptic levels. NMDA receptor (NMDAR)–dependent inhibitory long-term potentiation (iLTP) at GABAergic postsynapses requires an increase in surface $GABA_A$Rs through promoted exocytosis; however, the regulatory mechanisms and the neuropathological significance remain unclear. Here we report that the autism-related protein PX-RICS is involved in $GABA_A$R transport driven during NMDAR–dependent GABAergic iLTP. Chemically induced iLTP elicited a rapid increase in surface $GABA_A$Rs in wild-type mouse hippocampal neurons, but not in *PX-RICS/RICS*–deficient neurons. This increase in surface $GABA_A$Rs required the PX-RICS/GABARAP/14–3-3 complex, as revealed by gene knockdown and rescue studies. iLTP induced CaMKII–dependent phosphorylation of PX-RICS to promote PX-RICS–14-3-3 assembly. Notably, *PX-RICS/RICS*–deficient mice showed impaired amygdala–dependent fear learning, which was ameliorated by potentiating GABAergic activity with clonazepam. Our results suggest that PX-RICS–mediated $GABA_A$R trafficking is a key target for GABAergic plasticity and its dysfunction leads to atypical emotional processing underlying autism.

1. Introduction

There is a growing consensus that autism arises from the atypical regulation of the excitation/inhibition balance within specific neural microcircuitry [1, 2]. In terms of neural inhibition, autism is closely related to dysfunctional inhibitory signaling mediated by the γ-aminobutyric acid (GABA) type A receptors ($GABA_A$Rs). Impaired presynaptic release of GABA and postsynaptic trafficking of $GABA_A$Rs lead to autistic-like social behavior in mouse models of autism [3–6]. There is a significant reduction in the number of $GABA_A$Rs and GABAergic activity in certain brain areas of autistic individuals [7–11]. Genetic association studies have revealed that several $GABA_A$R subunits are linked to an increased risk for autism [12–18]. $GABA_A$R–mediated signaling is thus essential for the proper regulation of the excitation/inhibition balance associated with socio-emotional cognition.

Similar to glutamatergic synapses, GABAergic synapses also exhibit activity–dependent plastic changes in their inhibitory transmission efficacy. Different forms of GABAergic synaptic plasticity based on diverse pre- and post-synaptic mechanisms have been characterized in different brain regions [19–22]. A major postsynaptic form of GABAergic synaptic plasticity is *N*-methyl-D-aspartate receptor (NMDAR)–dependent inhibitory long-term potentiation (iLTP) [21, 23–25], which is elicited by moderate stimulation of NMDARs that induces limited Ca^{2+} influx and preferential activation of Ca^{2+}/calmodulin–dependent protein kinase II (CaMKII). Activated CaMKII translocates to inhibitory synapses [26], where it triggers *de novo* $GABA_A$R transport to the neuronal surface, resulting in a persistent increase in the number of surface-expressed $GABA_A$Rs and inhibitory synaptic transmission. This increase in surface $GABA_A$Rs involves $GABA_A$R-associated protein (GABARAP), *N*-ethylmaleimide-sensitive factor (NSF) and glutamate receptor interacting protein (GRIP) [27]; however, the precise molecular mechanisms remain obscure. In particular, the relevant trafficking-related proteins that are phosphorylated by CaMKII and facilitate surface expression of $GABA_A$Rs are currently unidentified.

We have previously identified and characterized two splicing isoforms of GTPase-activating proteins specific for Cdc42 predominantly expressed in neurons of the cerebral cortex, amygdala and hippocampus: RICS (ARHGAP32 isoform 2) and PX-RICS (ARHGAP32 isoform 1) [28, 29]. RICS regulates NMDAR–mediated signaling at the postsynaptic density and axonal elongation at the growth cone [29, 30]. In contrast, PX-RICS forms an adaptor complex with GABARAP and 14-3-3ζ/θ to facilitate steady-state trafficking of the N-cadherin/β-catenin complex and $GABA_A$Rs [3, 28, 31, 32]. *PX-RICS* is also responsible for autistic-like features observed in more than half of the patients with Jacobsen syndrome (JBS) [3]. Mice lacking *PX-RICS/RICS* show marked decreases in surface-expressed $GABA_A$Rs and $GABA_A$R–mediated inhibitory synaptic transmission, resulting in various autistic-like behaviors

* Corresponding author.
E-mail address: nakamurachibiko@gmail.com (T. Nakamura).

https://doi.org/10.1016/j.ebiom.2018.07.011

and autism-related comorbidities [3]. Rare single-nucleotide variations in *PX-RICS* are also linked to non-syndromic autism, schizophrenia and alexithymia [33–35]. These findings strongly suggest that dysfunction of PX-RICS–mediated $GABA_AR$ trafficking has severe effects on socio-emotional processing of the brain.

Our previous study described above showed that PX-RICS and other components of the $GABA_AR$ trafficking complex are required for constitutive transport of the receptor. In this study, we have focused on the role of PX-RICS in the activity–induced promotion of $GABA_AR$ trafficking during iLTP. Here we show that PX-RICS–mediated $GABA_AR$ trafficking is also involved in NMDAR activity–dependent trafficking of $GABA_ARs$ and that PX-RICS is a key target of CaMKII for regulating GABAergic synaptic plasticity. Furthermore, we show that PX-RICS dysfunction in mice leads to impaired amygdala–dependent emotional learning, which manifests as autistic-like social behavior [3].

2. Materials and Methods

2.1. Mice

All animal experiments were reviewed and approved by the University of Tokyo Institutional Animal Care and Use Committee and were conducted according to the University of Tokyo Guidelines for Care and Use of Laboratory Animals. Mice were housed in clean plastic cages (CLEA Japan) lined with paper bedding (Japan SLC) at a constant temperature of 23 °C with a 12-h light/dark cycle (lights off at 21:00), with food and water available *ad libitum*. *PX-RICS*/*RICS*–deficient mice were generated as described [30]. Mutant mice were backcrossed into the C57BL/6 N (CLEA Japan) background until the F10 generation. The mice used in behavioral studies were generated by breeding heterozygous mutant males and females in the C57BL/6 N background. Adult and young-adult male mice (20 and 8–10 weeks old, respectively) from a naïve cohort were used in the fear conditioning and pain sensitivity tests. The embryos for primary neuronal cultures were generated by crossing wild-type C57BL/6 N males and females, or homozygous mutant males and females in the C57BL/6 N background. Embryonic day (E) 16–18 embryos were used for primary culture of hippocampal neurons.

PX-RICS/*RICS*–deficient mice carry the disrupted *Arhgap32* gene encoding PX-RICS and RICS, two splicing isoforms with the distinct cellular functions [3, 28, 29, 31, 32]. Autistic-like behaviors of the mutant mice are reversed by a $GABA_AR$ agonist clonazepam, suggesting that these phenotypes are caused by PX-RICS dysfunction, not by RICS deficiency [3]. For this reason, the KO mice were termed *PX-RICS* KO in our previous studies. In this study, however, the KO mice were accurately termed *PX-RICS*/*RICS* KO.

2.2. Cell Culture and Transfection

Hippocampal neurons were isolated from E16–18 mouse embryos and plated on 24-well tissue culture plates precoated with 1 mg/ml poly-L-lysine (Sigma-Aldrich) as described [29]. Cells were cultured in Neurobasal medium (Thermo Fisher Scientific) supplemented with B-27 supplement (Thermo Fisher Scientific) and 0.5 mM L-glutamine (Thermo Fisher Scientific). For the first 3 days in culture, 10 μM cytosine β-D-arabinofuranoside (Ara-C; Sigma-Aldrich) was included in the culture medium. Half of the medium was changed every 3 days. Transfection of primary cultured neurons was performed at 14 days *in vitro* (DIV) using FuGENE 6 (Roche) for plasmid constructs and 10 DIV using Lipofectamine RNAiMAX (Thermo Fisher Scientific) for siRNAs. Three hours after transfection, the medium was replaced with conditioned medium.

2.3. Chem-iLTP Induction

Induction of chem-iLTP was performed as described [27]. Briefly, mouse hippocampal neurons in culture were treated with 20 μM NMDA (Sigma-Aldrich) plus 10 μM 6-cyano-7-nitroquinoxaline-2,3-dione (CNQX; Sigma-Aldrich) for 3 min at 37 °C followed by recovery incubation in conditioned medium for 12 min at 37 °C. The cell-permeable, water-soluble CaMKII inhibitor KN93 [36] (1 μM; Merck Millipore) was applied for 30 min prior to NMDA treatment and also was added to the medium for NMDA stimulation and for recovery incubation. Neurons were then subjected to immunoblotting, immunoprecipitation or surface labeling.

2.4. Antibodies

A rabbit polyclonal antibody (pAb) against PX-RICS was generated as described [28]. A rabbit pAb specific for the $GABA_AR$ β3 subunit phosphorylated at Ser^{383} (phospho-S^{383}) was a kind gift from Dr. Stephen J. Moss (Department of Neuroscience, Tufts University School of Medicine) [37, 38]. Commercially available antibodies used for immunoblotting were as follows: rabbit monoclonal antibody (mAb) against CaMKII (1:1000; Cell Signaling Technology, #4436, lot: 3), rabbit mAb against phospho-CaMKII (Thr^{286}) (1:1000; Cell Signaling Technology, #12716, lot: 3), rabbit pAb against GluA1 (1:600; Abcam, ab31232, lot: GR79640-1), rabbit pAb against phospho-GluA1 (Ser^{845}) [1:500; Upstate Biotechnology, #06-773 (currently AB5849, Merck Millipore), lot: 23869A], mouse mAb against α-tubulin (1:500; Merck Millipore, CP06, lot: D00160163), rabbit pAb against 14-3-3ζ (1:100; Santa Cruz Biotechnology, sc-1019, lot: C1008), mouse mAb against 14-3-3θ (1:5000; Sigma-Aldrich, T5942, lot: 107 K1655), and mouse mAb against $GABA_AR$ β3 subunit (1:1000; Synaptic Systems, #224411, lot: 224411/1). Commercially available antibodies used for immunofluorescent staining were as follows: rabbit pAb against the $GABA_AR$ γ2 subunit (1:500; Synaptic Systems, #224003, lot: 224003/8) and mouse mAb against vesicular GABA transporter (VGAT) (1:1000; Synaptic Systems, #131011, lot: 131011/26).

2.5. Immunoprecipitation and Immunoblotting

Mouse hippocampal neurons (14 DIV) were lysed in lysis buffer T [10 mM Tris-HCl (pH 6.8), 140 mM NaCl, 1 mM EDTA, 1% Triton X-100 with protease/phosphatase inhibitor cocktail (Sigma-Aldrich)]. The lysates were precleared with protein A–Sepharose (GE Healthcare) for 1 h at 4 °C. Precleared lysates (500 μg of protein) were incubated with 5 μg of the indicated antibody for 1 h at 4 °C, and then the immunocomplexes were adsorbed to protein A–Sepharose for 1 h at 4 °C. After being washed extensively with lysis buffer T, the immunoprecipitates were resolved by SDS-PAGE and transferred to a polyvinylidene difluoride membrane (Merck Millipore). The blots were probed with primary antibodies as indicated and visualized with alkaline phosphatase–conjugated secondary antibodies (Promega). Band intensities were quantified using ImageJ software.

2.6. Phos-tag SDS-PAGE

Phos-tag SDS-PAGE [6% acrylamide containing 50 μM Phos-tag acrylamide (Wako)] and immunoblotting were performed according to the manufacturer's instructions.

2.7. Labeling of Surface and Internal γ2 Subunits

Surface labeling was performed as described [3]. The rabbit pAb against γ2 (Synaptic Systems) used for surface labeling recognizes the N-terminal extracellular region of the subunit. Briefly, primary and secondary antibodies used for surface labeling before fixation were diluted in conditioned medium from 14 DIV hippocampal neurons. Mouse hippocampal neurons (14 DIV) were surface-labeled with anti–γ2 (1:500) for 30 min at room temperature and rinsed in phosphate-buffered saline (PBS). The neurons were then incubated with Alexa Fluor 488–conjugated anti–rabbit IgG (1:500; Thermo Fisher Scientific) for

30 min at room temperature and rinsed in PBS. After being fixed with 2% paraformaldehyde in PBS for 15 min at room temperature, the neurons were incubated with unconjugated anti–rabbit IgG (50 μg/ml; Sigma-Aldrich) for 1 h at room temperature to block the unlabeled primary antibody remaining on the neuronal surface, rinsed in PBS and then permeabilized with 0.2% Triton X-100 in PBS for 5 min. The neurons were again incubated with anti–γ2 for 60 min at room temperature, followed by staining with Alexa Fluor 594– or Alexa Fluor 647–conjugated anti–rabbit IgG (1:500; Thermo Fisher Scientific) for 60 min at room temperature. Alternatively, in Fig. 3, the neurons were double-stained with anti–γ2 and mouse mAb against FLAG (M2; 1:500; Sigma-Aldrich), and then with Alexa Fluor 647–labeled anti–rabbit IgG and Alexa Fluor 594–labeled anti–mouse IgG. The cell images were obtained with an LSM510META laser scanning confocal microscope (ZEISS). The settings of the microscope, lasers and detectors were kept constant during image acquisition. The surface-expressed γ2 levels were quantitatively evaluated by analyzing fluorescent images with ImageJ software. The validity of this surface labeling protocol was confirmed in our previous report [3]. To exclude the possibility of artificial aggregation of surface $GABA_A$Rs, the results obtained by two distinct labeling methods were quantitatively compared (see Supplementary Fig. 1).

2.8. siRNA–Mediated Gene Silencing

Primary cultured mouse neurons (10 DIV) were transfected with siRNAs (10 nM) plus Red Fluorescent Oligo (10 nM; Thermo Fisher Scientific) using Lipofectamine RNAiMAX according to the manufacturer's protocol. Three hours after transfection, the medium was replaced with conditioned medium. The silencing effect was evaluated by immunofluorescence 96 h after transfection. Surface labeling of siRNA-transfected neurons was performed as described above. The sequences for stealth RNAi siRNAs (Thermo Fisher Scientific) were as follows:

siGabarap-1, 5′-AAACAAGGCAUCUUCAGCACGGAGA-3′;
siGabarap-2, 5′-AAAGAAGUCUUCUUCAUGGUGUUCC-3′;
si14-3-3ζ-1, 5′-UUGAGGGCCAGACCCAGUCUGAUGG-3′;
si14-3-3ζ-2, 5′-UUUGCAAGAGAGCAGGCUUUCUCUG-3′;
si14-3-3θ-1, 5′-AGAGGUGUCGGUCUUCUGCUCAAUG-3′;
si14-3-3θ-2, 5′-AUCAAACGCCUCUUGGUAGGCUCCU-3′;
siDctn1-1, 5′-UUAACUCCUUGAUAACUGUCUCUCG-3′ and
siDctn1-2, 5′-UGCCCAUGUAGACUGUGUCAUCUUG-3′.

Stealth RNAi negative control medium GC duplex (Thermo Fisher Scientific) is denoted as siControl in the figures.

2.9. PX-RICS Mutants

PX-RICS mutants were generated by PCR-based mutagenesis [39, 40]. PX-RICS-ΔGBR, a mutant lacking the GABARAP–binding region (amino acids 562–796); PX-RICS-ΔRSKSDP, a mutant lacking the 14-3-3–binding motif (amino acids 1793–1798); PX-RICS-S1796A, a mutant in which Ser^{1796}, the CaMKII phosphorylation site in the 14-3-3 binding motif, was replaced with Ala. These mutants were cloned in frame into the mammalian expression vector pcDNA3.1(+)-FLAG.

2.10. Fear Conditioning Test

WT and KO littermates [20-week-old male mice; 32.10 ± 1.06 g (WT); 32.20 ± 1.00 g (KO)] were assessed for learning and memory of conditioned fear in accordance with previous reports [41, 42]. The experiments were conducted using a computer-controlled fear-conditioning system (O'HARA & CO., LTD). Either of two test boxes with different contextual (visual, tactile and olfactory) cues were placed in a soundproof chamber (60 × 45 × 60 cm). A transparent Plexiglas box (10 × 10 × 12 cm, inside dimensions) with a transparent lid was used in context 1. The floor was made up of 14 stainless steel bars (0.2 cm in diameter) set 0.5 cm apart, which served as conductors of electric footshocks. The box was placed in a white-surrounding environment (60 lx), and background fan noise (50 dB) was provided during context 1 experiments. The context 1 test box was cleaned of odors with 70% ethanol and wiped with paper towels before each conditioning or contextual test. In context 2, a white opaque polycarbonate box of the identical size with a smooth floor containing 1-cm-thick paper bedding was placed in a black-surrounding environment (15 lx), and louder background fan noise (60 dB) was provided during the experiments. The test box was cleaned with water and air-dried before each cued test. Paper bedding was replaced before each cued test.

The procedures for the conditioning and test sessions are illustrated schematically in Fig. 5A. Test mice were habituated to the testing room for at least 24 h before beginning the test. On the first day, a test mouse was placed in the test box (context 1) and allowed to explore freely for 120 s. The mouse was then exposed to a 30-s tone of 70 dB (CS), which co-terminated with a 2-s electric footshock of 0.75 mA (US). After a 30-s post-shock exploration, the mouse was immediately returned to its home cage. Context–dependent fear learning was tested on the second day, 24 h after the conditioning. Each mouse was placed back in the context 1 test box, and freezing behavior was monitored for 300 s in the absence of the CS and US. After an interval of 2 h, the mice were placed in the altered context (context 2), and cued fear learning was tested. The session consisted of a 120-s free exploration, followed by a 180-s continuous presentation of the identical CS tone, and the freezing behavior in response to the altered context (pre-CS phase) or the tone (CS phase) was assessed for 300 s in total. Movements of animals were automatically recorded at the rate of 2 frames/s and analyzed with a video-tracking system. Behavioral activity was defined as the area through which an animal moved (in pixels) between two consecutive frames, and freezing behavior was defined as an absence of movement (≤30 pixels) maintained for >1 s.

2.11. Pain Sensitivity Test

Pain sensitivity flinch/jump test was conducted as described [43, 44]. WT and KO males (20 weeks old) from a naive cohort were placed in the test box (context 1) and habituated for 120 s. Each mouse received 1-s electric footshocks of varying intensity: the intensity was increased by 0.02 mA every 20 s, with an initial footshock of 0.02 mA. The minimal current intensity required to elicit stereotyped aversive responses, such as flinching, vocalization and running/jumping, was measured for each mouse. The experiment was discontinued when the test mouse exhibited all three responses. The test box was cleaned of odors with 70% ethanol and wiped with paper towels between tests.

2.12. CZP Treatment

CZP (Wako) was suspended in vehicle solution [0.5% (w/v) methylcellulose 400 (Wako) in PBS] and diluted with additional vehicle solution for injection to a volume of 10 ml/kg at a dose of 0.03 mg/kg. Our previous study indicated that intraperitoneal administration of CZP at a dose of up to 0.03 mg/kg causes no significant sedative or anxiolytic effects in either WT or KO mice [3], which allows us to avoid secondary effects that could potentially affect their learning performance. The diluted CZP suspension or vehicle solution was intraperitoneally administered to each test mouse (male, 8–10 weeks old) 30 min before conditioning. Contextual and cued tests of the vehicle- or CZP-injected mice were performed as described above.

2.13. Statistical Analysis

All experiments were carried out by individuals who were blind to the genotypes and/or treatments. Sampling and experimental replicates in cell biological analyses are described in the figure legends. No criteria were applied for inclusion or exclusion of data. No outliers were taken into account and all collected data were subjected to statistical analyses. All data are represented as the mean ± SEM. and were analyzed using Student's *t*-test, one-way analysis of variance (ANOVA), and two-way

ANOVA with Bonferroni's *post hoc* test. All the statistical analyses were performed using js-STAR software. Full statistical data for the behavioral tests are presented in Supplementary Table 1.

3. Results

3.1. iLTP Triggers PX-RICS–Dependent $GABA_AR$ Transport

We first examined whether PX-RICS is responsible for the increase in surface $GABA_ARs$ underlying NMDAR–dependent GABAergic iLTP. To induce this type of iLTP, we adopted a chemical method (chem-iLTP) based on moderate stimulation of NMDARs with low-dose NMDA in cultured hippocampal neurons (see Materials and Methods and Supplementary Fig. 2) [27, 45–47]. The γ2 subunit is estimated to be present in ~90% of the $GABA_AR$ complexes in the brain [48], and we thus assessed the surface and intracellular γ2 levels after the chem-iLTP induction. Compared with mock-treated *PX-RICS*$^{+/+}$ (WT) neurons, NMDA-treated WT neurons showed a rapid increase in surface γ2 levels, and this increase was clearly inhibited by pretreatment with KN93, a cell-permeable, water-soluble CaMKII inhibitor (Fig. 1A and Supplementary Fig. 3A). In contrast, as shown in our previous report [3], mock-treated *PX-RICS*$^{-/-}$ (KO) neurons exhibited markedly lower surface γ2 levels

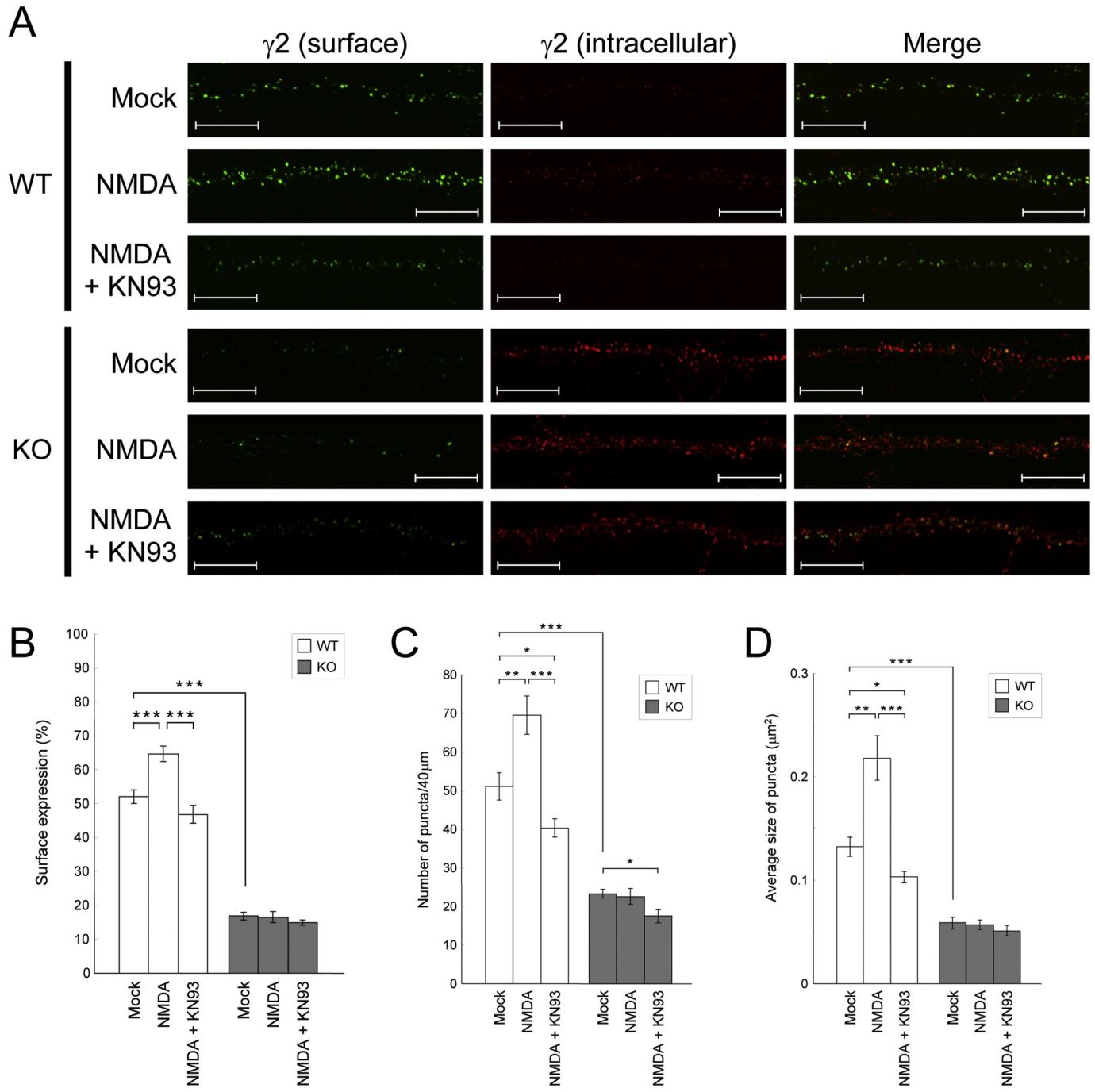

Fig. 1. PX-RICS is required for $GABA_AR$ transport during chem-iLTP. (A) WT and KO hippocampal neurons were treated with vehicle (mock) or moderately stimulated with NMDA in the presence or absence of KN93 as indicated, and surface (green) and intracellular (red) γ2 subunits were separately visualized. Scale bars, 10 μm. (B–D) Quantitative analyses of the γ2 fluorescent signals in the distal dendrites (B). The number (C) and averaged size (D) of surface-expressed γ2 puncta within a 40-μm segment of the representative dendrites were also quantified. Data are shown as the mean ± SEM. $^*P < .05$; $^{**}P < .01$; $^{***}P < .001$ (Student's *t*-test). $n = 10$ (WT) and 10 (KO) across two independent experiments. See also Supplementary Fig. 3

than did mock-treated WT neurons (Fig. 1A and Supplementary Fig. 3A), suggesting that PX-RICS is required for steady-state transport under the unstimulated condition. Notably, the surface γ2 levels of KO neurons remained unchanged even after NMDA stimulation (Fig. 1A and Supplementary Fig. 3A). Quantitative analysis of the fluorescence intensities and dendritic fluorescent puncta revealed that NMDA stimulation induced 25–65% increase in the surface expression and in the number and size of the dendritic γ2 puncta in WT neurons, whereas no significant changes were found in KO neurons (Fig. 1B–D and Supplementary Fig. 3B). These results suggest that PX-RICS is required for CaMKII–dependent transport of $GABA_A$Rs to the neuronal surface during chem-iLTP.

3.2. $GABA_AR$ Transport During iLTP Requires the PX-RICS–Mediated Trafficking Complex

We next investigated whether components of the PX-RICS–mediated trafficking complex are required for the NMDA–induced increase in surface $GABA_A$Rs. In WT neurons transfected with a control small interfering RNA (siRNA), the surface γ2 levels increased after NMDA stimulation (Fig. 2 and Supplementary Figs. 4 and 5). As shown in our previous report [3], introduction of an siRNA targeting any one of GABARAP, 14-3-3ζ, 14-3-3θ or dynactin1 resulted in a drastic reduction in surface γ2 levels and a simultaneous increase in intracellular γ2 levels in mock-treated WT neurons (Fig. 2 and Supplementary Figs. 4 and 5). Furthermore, siRNA-transfected WT neurons showed no significant increase in surface-expressed γ2 after NMDA stimulation (Fig. 2 and Supplementary Figs. 4 and 5). These results suggest that GABARAP, 14-3-3ζ, 14-3-3θ and dynactin1 are essential for $GABA_A$R surface expression triggered by chem-iLTP induction.

We further studied the importance of PX-RICS–mediated complex formation by using mutant forms of PX-RICS: ΔGBR, a mutant lacking the GABARAP-binding region, and ΔRSKSDP and S1796A, mutants lacking the ability to bind 14-3-3 (Fig. 3 and Supplementary Fig. 6). When WT PX-RICS was exogenously expressed in KO neurons, the surface γ2 levels were restored under the unstimulated condition and further increased by NMDA stimulation (Fig. 3 and Supplementary Fig. 6). In contrast, KO neurons transfected with the ΔGBR mutant exhibited notably lower surface γ2 levels and no further enhancement of γ2 surface expression after NMDA stimulation. Similarly, surface γ2 levels remained unchanged in KO neurons expressing either the ΔRSKSDP or S1796A mutant (Fig. 3 and Supplementary Fig. 6). Taken together, these results suggest that $GABA_A$R trafficking newly driven during chem-iLTP requires the formation of the PX-RICS/GABARAP/14–3-3 complex.

3.3. CaMKII Targets PX-RICS to Stimulate $GABA_AR$ Transport During iLTP

In NMDAR–dependent GABAergic iLTP, CaMKII phosphorylates target proteins such as gephyrin and the $GABA_A$R β3 subunit to stimulate $GABA_A$R surface expression [21, 23–25, 37, 38, 49]. *In vitro*, CaMKII directly phosphorylates PX-RICS at Ser^{1796} to generate a 14-3-3–binding motif (-RSKpSDP-), thereby promoting the interaction of PX-RICS with 14-3-3 proteins [31]. We thus determined whether PX-RICS is one of the CaMKII targets relevant to GABAergic iLTP. Phos-tag SDS-PAGE and subsequent quantitative analyses revealed that NMDA treatment of WT neurons decreased the electrophoretic mobility of PX-RICS, and this decrease was alleviated by pretreatment of neurons with KN93 (Fig. 4A). In addition, NMDA stimulation increased the amount of 14-3-3ζ/θ bound to PX-RICS, and this increase was abrogated in the presence of KN93 (Fig. 4B). Collectively, we concluded that NMDAR activation elicits CaMKII–dependent phosphorylation of PX-RICS to enhance the recruitment of 14-3-3ζ/θ to PX-RICS, thereby driving *de novo* surface expression of $GABA_A$Rs. The PX-RICS/GABARAP/14-3-3 adaptor complex is thus considered to be an essential molecular target for inducing GABAergic iLTP.

CaMKII-dependent phosphorylation at Ser^{383} of the $GABA_A$R β3 subunit promotes gephyrin accumulation and $GABA_A$R immobilization at synapses during chem-iLTP [37]. We examined whether this regulatory mechanism downstream of β3-Ser^{383} phosphorylation operates normally regardless of PX-RICS. We found that β3-Ser^{383} phosphorylation is induced during chem-iLTP in both WT and *PX-RICS/RICS* KO neurons and there is no significant difference in the phosphorylation rate between both genotypes (Fig. 4C). This result suggests that the synaptic recruitment and confinement of $GABA_A$Rs are properly regulated through β3-Ser^{383} phosphorylation independently of PX-RICS. We then assessed changes in synaptic and nonsynaptic localization of $GABA_A$Rs during chem-iLTP in WT neurons. As expected, chem-iLTP significantly increased synaptic $GABA_A$Rs (Fig. 4D) probably through β3-Ser^{383} phosphorylation. Interestingly, we found that nonsynaptic $GABA_A$Rs is also significantly increased to the same degree (Fig. 4D). Taken together, these results support that anterograde transport and/or membrane insertion of $GABA_A$Rs are promoted during chem-iLTP.

3.4. Amygdala–Dependent Fear Learning is Impaired in PX-RICS/RICS–Deficient Mice

The amygdala plays a key role in processing emotional memories, particularly those associated with fear [50, 51], and its dysfunction is implicated in autism pathogenesis [52, 53]. Fear conditioning is inversely correlated with the severity of autism [54–56] and depends on GABAergic activity and plasticity within the amygdala [41, 42, 57]. To explore a link between PX-RICS–dependent GABAergic plasticity and autism, we conducted a fear conditioning test of *PX-RICS/RICS* KO mice (Fig. 5A).

During the conditioning period, WT and KO mice were similarly active before the tone (conditioned stimulus; CS)–shock (unconditioned stimulus; US) pairs (Fig. 5B) and showed similar levels of freezing response (Fig. 5C). Similarly, WT and KO mice showed similar averaged freezing rates and time courses during contextual testing (Fig. 5D–E), although KO mice had a tendency to freeze less frequently, indicating that there is little difference in context–dependent fear learning. In cued testing, however, KO mice showed a significantly reduced freezing response to the tone (CS) (Fig. 5F). Time course analysis revealed that there was no significant difference in the freezing rates before tone presentation (pre-CS phase) (Fig. 5G). The freezing response of WT mice was significantly increased at the start of tone presentation (CS phase) and was consistently higher thereafter (Fig. 5G). In contrast, KO mice showed less increase in the freezing rate between pre-CS and CS phases (Fig. 5G). As a result, KO mice consistently showed much lower levels of freezing behavior than did WT mice during the CS phase, suggesting that KO mice are markedly inferior to WT mice in tone-cued fear learning. PX-RICS is thus required for cued fear learning, which is believed to depend critically on emotional functions of the amygdala.

Subsequent pain sensitivity tests, as measured by responses to footshocks of varying intensity, revealed that there were no significant differences in the minimal current intensity required to elicit stereotyped aversive responses (Fig. 5H). Therefore, the observed difference in the post-tone freezing rate was not attributed to potential differences in pain sensitivity but to differences in the ability of the amygdala to form fear memory. These results suggest that PX-RICS–dependent GABAergic plasticity plays critical roles in emotional learning in the amygdala, and hence its impairment contributes to atypical socio-emotional processing that manifests as autistic-like social behavior.

3.5. Potentiating $GABA_AR$–Mediated Signaling Ameliorates Fear Learning

We have previously shown that autistic-like behavior in *PX-RICS/RICS* KO mice is treatable by potentiating postsynaptic signaling through the $GABA_A$Rs remaining on the neuronal surface with clonazepam (CZP), a benzodiazepine agonist of $GABA_A$Rs [3]. We thus

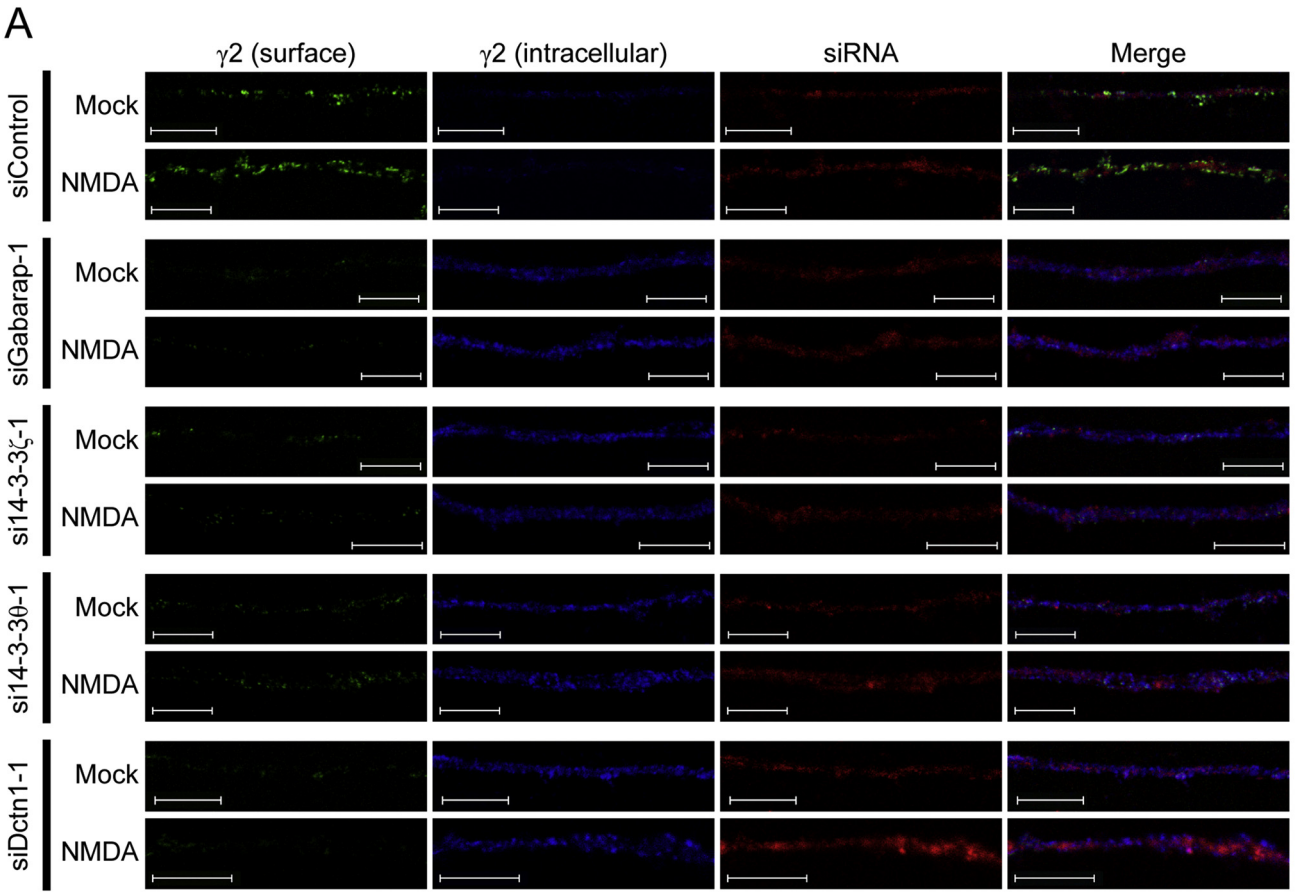
A
γ2 (surface)
γ2 (intracellular)
siRNA
Merge
siControl
siGabarap-1
si14-3-3ζ-1
si14-3-3θ-1
siDctn1-1
Mock
NMDA

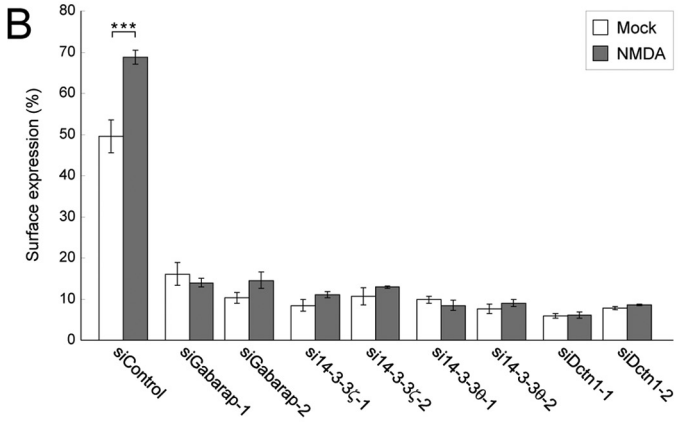
B
Surface expression (%)
***
Mock
NMDA
siControl
siGabarap-1
siGabarap-2
si14-3-3ζ-1
si14-3-3ζ-2
si14-3-3θ-1
si14-3-3θ-2
siDctn1-1
siDctn1-2

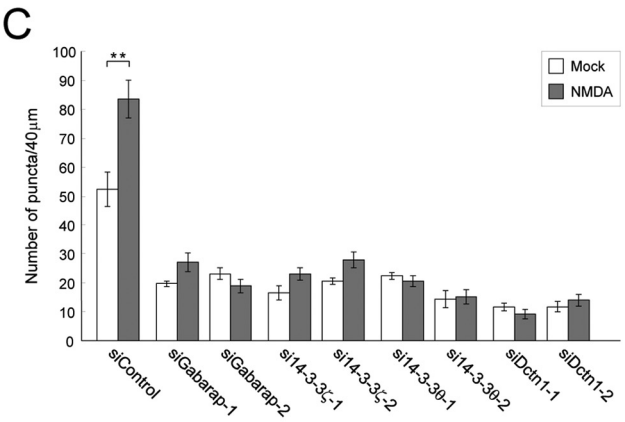
C
Number of puncta/40μm
**
Mock
NMDA
siControl
siGabarap-1
siGabarap-2
si14-3-3ζ-1
si14-3-3ζ-2
si14-3-3θ-1
si14-3-3θ-2
siDctn1-1
siDctn1-2

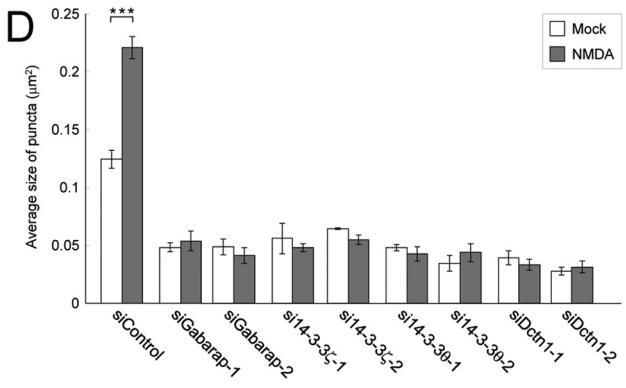
D
Average size of puncta (μm²)
***
Mock
NMDA
siControl
siGabarap-1
siGabarap-2
si14-3-3ζ-1
si14-3-3ζ-2
si14-3-3θ-1
si14-3-3θ-2
siDctn1-1
siDctn1-2

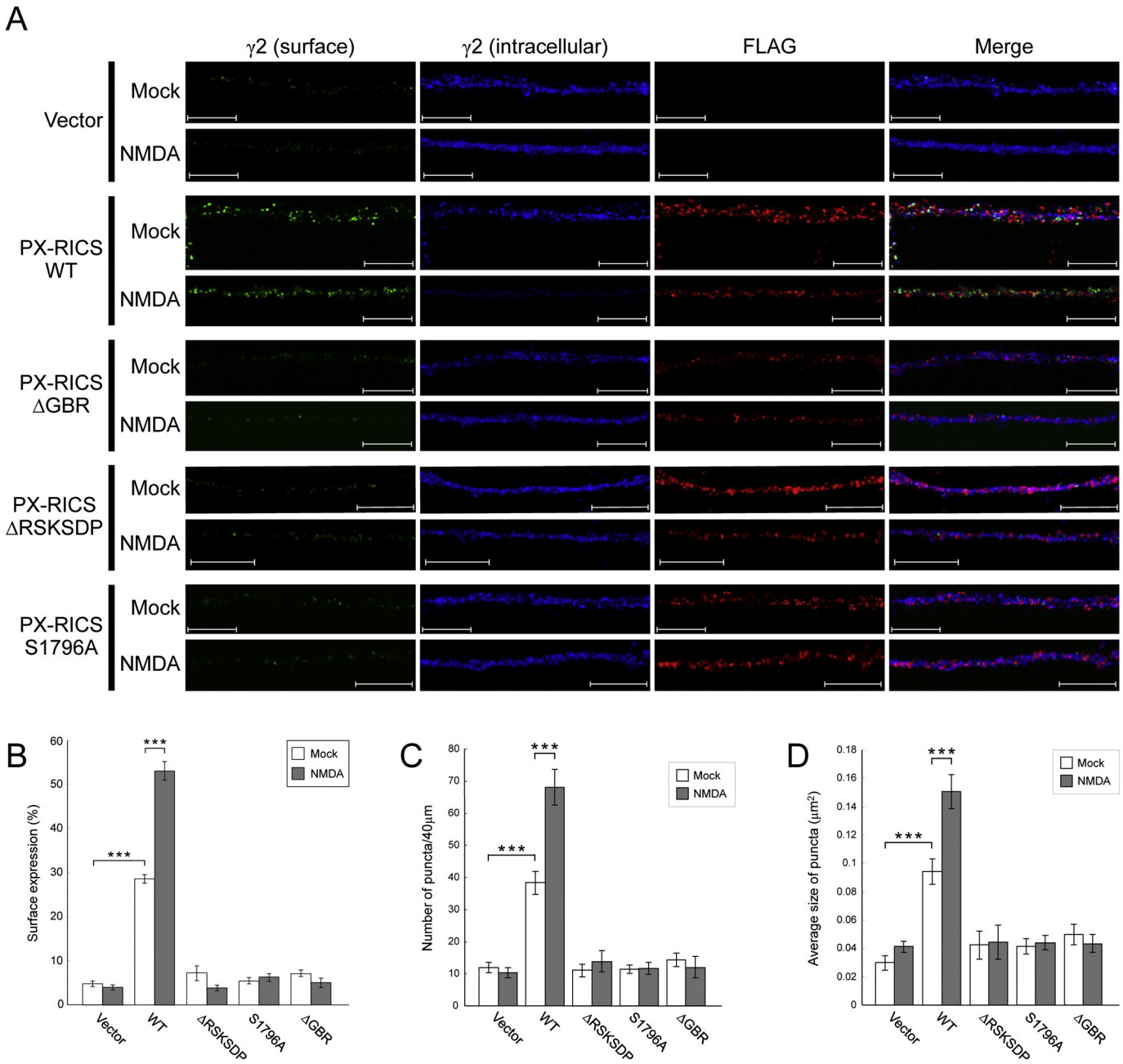

Fig. 3. $GABA_AR$ transport during chem-iLTP requires complex formation of PX-RICS with GABARAP and 14-3-3ζ/θ. (A) KO hippocampal neurons were transfected with plasmids expressing FLAG-tagged wild-type or mutant PX-RICS as indicated. After mock or moderate NMDA stimulation, surface-expressed (green) and intracellular (blue) levels of the γ2 subunit in the distal dendrites of transfected neurons (red) were analyzed. Scale bars, 10 μm. (B–D) Quantitative analyses of γ2 fluorescent signals (B). The number (C) and averaged size (D) of surface-expressed γ2 puncta within a 40-μm segment of the representative dendrites were also quantified. Data are shown as the mean ± SEM. $^{***}P < 0.001$ (Student's *t*-test). $n = 10$ (for each construct) across two independent experiments. See also Supplementary Fig. 6.

analyzed whether fear learning of *PX-RICS/RICS* KO mice could be ameliorated by CZP treatment. Intraperitoneal administration of CZP at a dose of 0.03 mg/kg caused no significant effects on locomotor activity or freezing behavior in either WT or KO mice during the conditioning session (Fig. 6A–B), as we showed in our previous study [3]. Vehicle- and CZP-injected mice showed similar levels of freezing behavior during contextual testing, although CZP had a marginal ameliorating effect in KO mice (Fig. 6C–D). In cued testing, there was no apparent difference in the freezing rates during the pre-CS phase (Fig. 6E–F). In the CS phase, however, CZP-treated KO

Fig. 2. GABARAP, 14-3-3ζ/θ and dynactin1 are required for $GABA_AR$ transport during chem-iLTP. (A) WT hippocampal neurons were transfected with the indicated siRNA plus Red Fluorescent Oligo. After treatment with vehicle (mock) or low-dose NMDA, surface (green) and intracellular (blue) levels of the γ2 subunit in the distal dendrites of siRNA-transfected neurons (red) were analyzed. Scale bars, 10 μm. (B–D) Quantitative analyses of γ2 fluorescent signals (B). The number (C) and averaged size (D) of surface-expressed γ2 puncta within a 40-μm segment of the representative dendrites were also quantified. Data are shown as the mean ± SEM. $^{**}P < 0.01$; $^{***}P < 0.001$ (Student's *t*-test). $n = 10$ (for each siRNA) across two independent experiments. See also Supplementary Figs. 4 and 5.

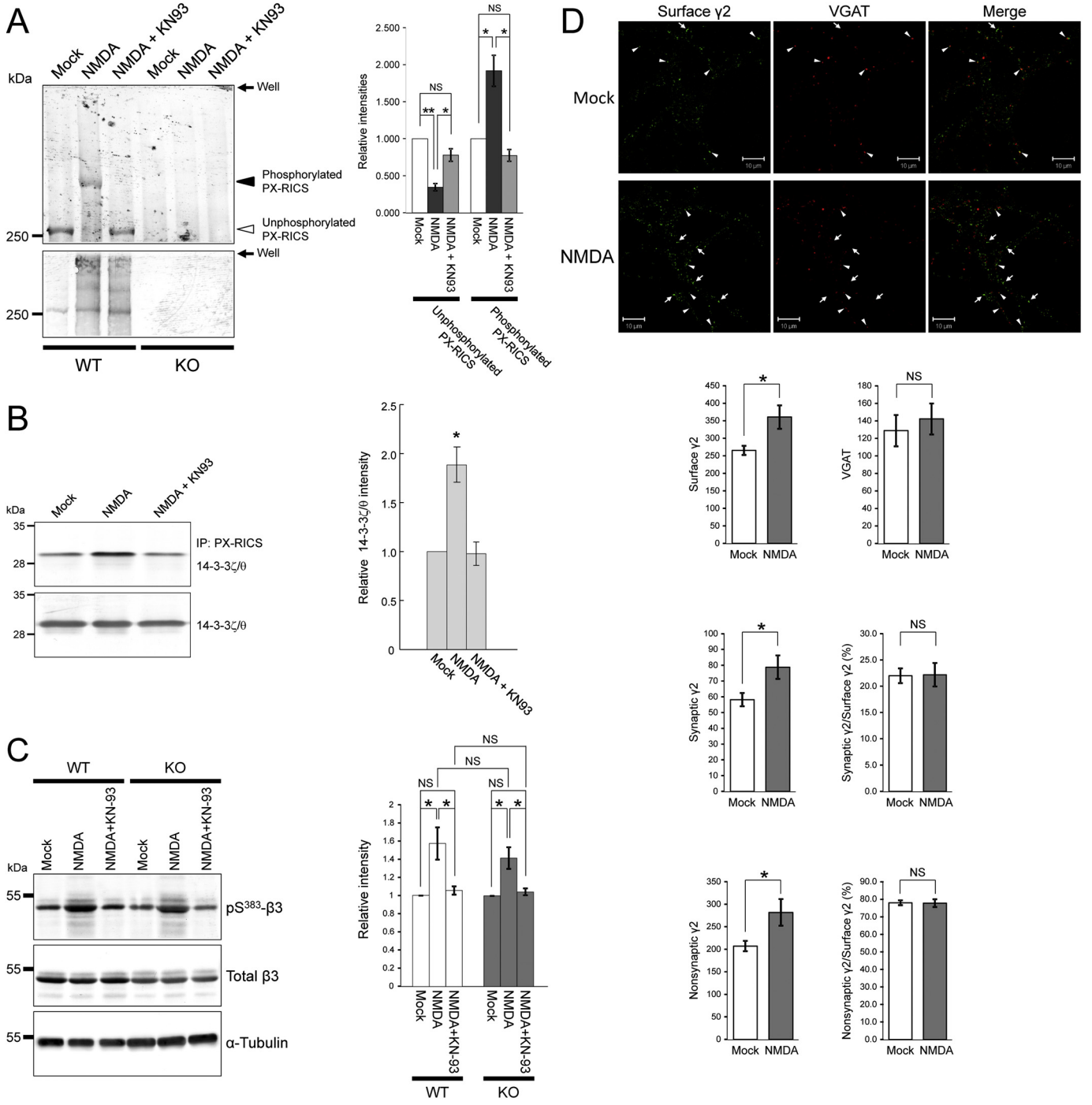

Fig. 4. Chem-iLTP induces CaMKII–dependent PX-RICS phosphorylation to promote the assembly of PX-RICS and 14-3-3 and cell surface transport of $GABA_A$Rs. (A) WT and KO hippocampal neurons were moderately stimulated with NMDA in the presence or absence of KN93. The neuronal lysates were immunoprecipitated with an anti–PX-RICS antibody, and half of the immunoprecipitate was analyzed by Phos–tag (upper) or standard (lower) SDS-PAGE and immunoblotting. The intensities of unphosphorylated and phosphorylated PX-RICS bands (open and filled arrowheads, respectively) were corrected using those of total PX-RICS and the data were expressed as relative values with respect to the mock control (right panel). (B) WT hippocampal neurons were moderately stimulated with NMDA, and the lysates were analyzed by immunoprecipitation with an anti–PX-RICS antibody followed by immunoblotting with anti–14-3-3ζ and anti–14-3-3θ antibodies (upper panel). Total 14–3-3ζ/θ protein in the neuronal lysates was assessed by immunoblotting with anti–14-3-3ζ and anti–14-3-3θ antibodies (lower panel). Quantitative analysis of 14-3-3ζ/θ bound to PX-RICS (right panel). The ratio of the band intensity of 14-3-3ζ/θ bound to PX-RICS to that of total 14-3-3ζ/θ was assessed, and the data were expressed as relative values with respect to mock control. (C) Lysates of WT and KO hippocampal neurons modestly stimulated with NMDA in the presence or absence of KN93 were analyzed by immunoblotting with anti–β3 and anti–phospho-Ser^{383} β3 antibodies. α-tubulin was used as an internal control for the quantitative analysis. (D) WT hippocampal neurons were modestly stimulated with NMDA and subjected to live cell labeling of the surface γ2, followed by co-staining with anti-VGAT antibody to identify synaptically localized $GABA_A$Rs (arrowheads). Arrows indicate large or elongated puncta of nonsynaptic γ2 often observed in NMDA-treated neurons. Scale bars, 10 μm. $n = 5$ (mock) and 5 (NMDA) across two independent experiments. Data are shown as the mean ± SEM from three (A, B, C) or two (D) independent experiments. NS, not significant; $^*P < 0.05$; $^{**}P < 0.01$ (Student's *t*-test).

mice showed a significantly higher freezing response than did vehicle-treated KO mice (Fig. 6E–F). The ameliorating effect of CZP was particularly noticeable early in the CS phase (Fig. 6F). The freezing rate of CZP-treated KO mice was nearly equivalent to that of vehicle- or CZP-treated WT mice (Fig. 6E–F), indicating that the poor learning performance of KO mice is significantly alleviated by

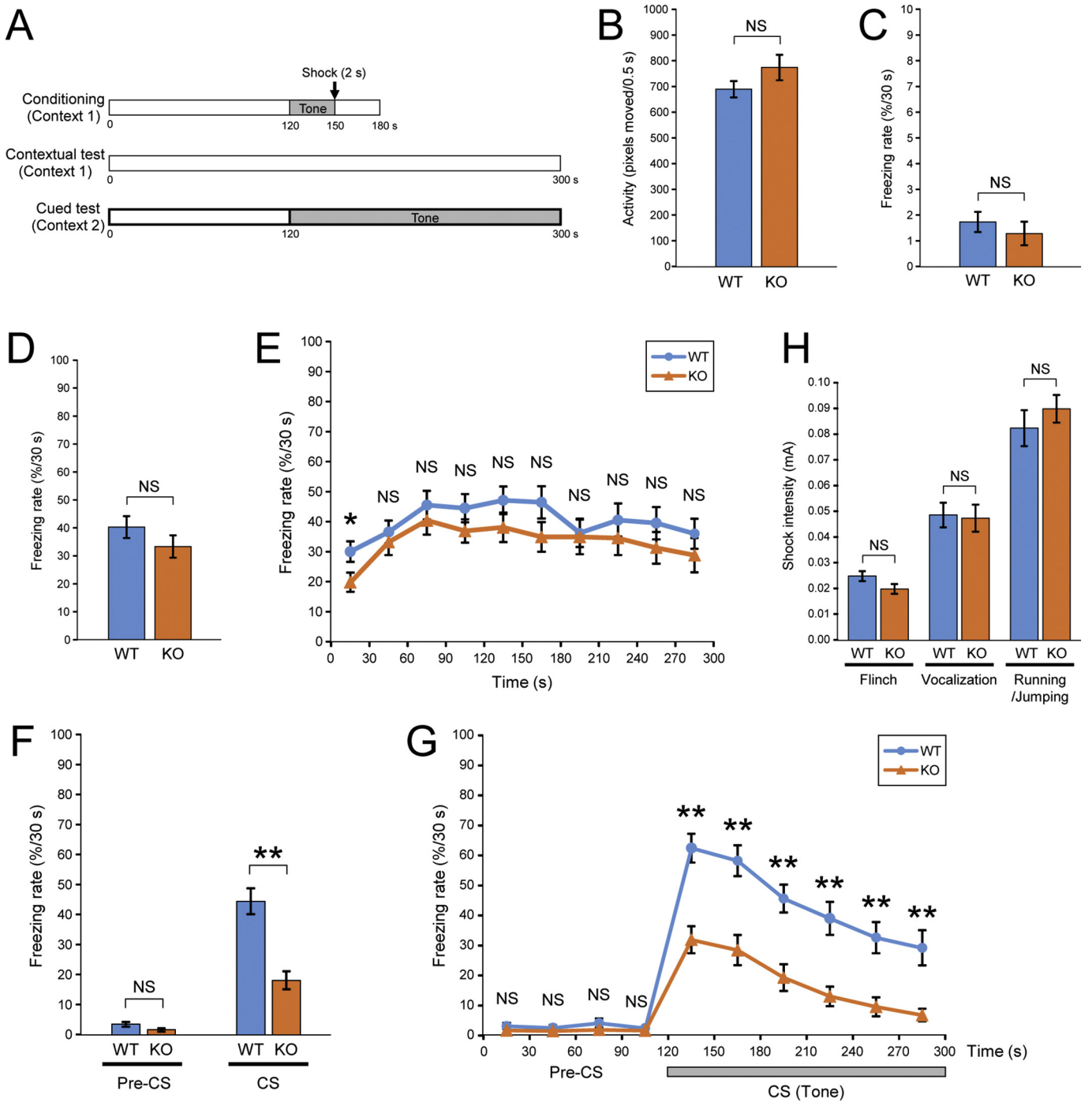

Fig. 5. Cued fear learning is impaired in *PX-RICS/RICS*–deficient mice. (A) Schematic diagram of the fear conditioning protocol. A conditioning session represents a single tone–footshock (CS–US) pair consisting of a 120-s free exploration, a 30-s tone presentation (gray bar), a 2-s electric footshock (arrow) and a 30-s post-tone period. A contextual test was performed for 300 s in the absence of the CS and US in an identical context. A cued test consisted of a 120-s pre-CS phase and a 180-s CS phase in an altered context. The percentage of the time spent freezing within a 30-s bin was defined as the freezing response. (B, C) WT and KO mice were assessed for activity (B) and averaged freezing rate (C) before tone presentation during the conditioning session. (D, E) Freezing responses during contextual tests were analyzed based on a 300-s bin (D) or in 30-s bins over the time course of the session (E). (F, G) Freezing responses were analyzed during the pre-CS and CS phases (F) and as a time course across these two phases (G). (H) The minimal current intensities of footshocks required to elicit the indicated aversive responses were measured in each mouse. Data are shown as the mean ± SEM. NS, not significant; $^{*}P < 0.05$; $^{**}P < 0.01$. $n = 26$ (WT) and 26 (KO) in (A–G); $n = 8$ (WT) and 8 (KO) in (H). Full statistical data are presented in Table S1.

CZP treatment. CZP had no significant effect on the freezing behavior of WT mice (Fig. 6C–F). These results suggest that the reduced ability of KO mice to form fear memory is caused by impaired postsynaptic $GABA_AR$–mediated signaling and that PX-RICS–dependent regulation of GABAergic activity is critical for emotional processing in the amygdala.

4. Discussion

Inhibitory synapses undergo several types of plasticity at both pre- and postsynaptic levels [19–22]. The postsynaptic form of plasticity at GABAergic synapses is achieved in part by modulating the intracellular and surface dynamics of $GABA_ARs$ in an activity–dependent manner

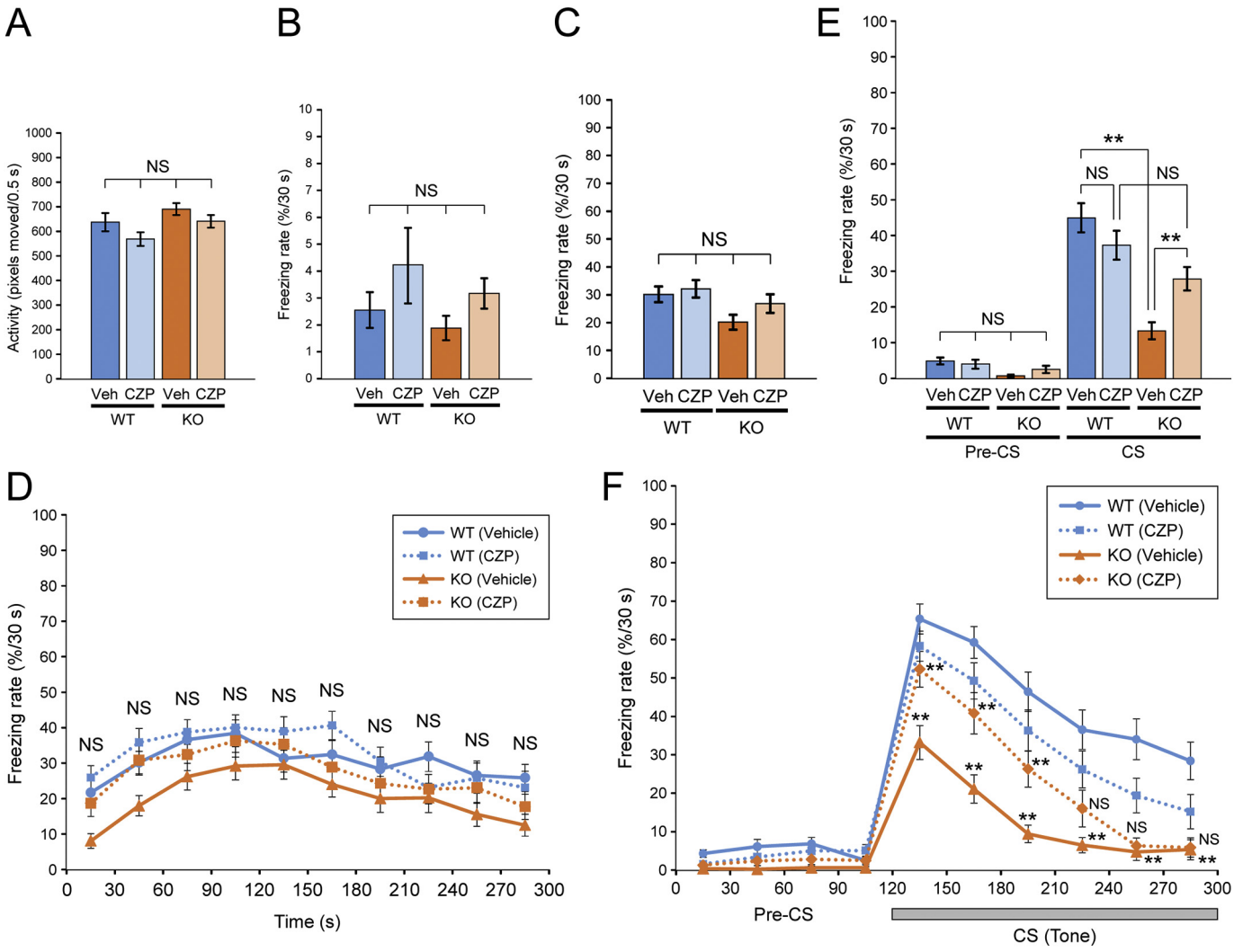

Fig. 6. Cued fear learning of *PX-RICS/RICS*–deficient mice is ameliorated by potentiating $GABA_AR$–mediated signaling. (A, B) Vehicle- and CZP-injected WT and KO mice were assessed for activity (A) and averaged freezing rate (B) before tone presentation during the conditioning session. (C, D) CZP has no significant effect on context–dependent fear learning. Freezing responses during contextual tests were analyzed based on a 300-s bin (C) or in 30-s bins over the time course of the session (D). (E, F) Freezing responses were analyzed during the pre-CS and CS phases (E) and as a time course across these two phases (F). CZP treatment produced significant improvement in the freezing response of KO mice during the CS phase (E), particularly early in the CS phase (F). Data are shown as the mean ± SEM. NS, not significant; $^{**}P < 0.01$. Comparisons between WT (Vehicle) and KO (Vehicle) and between KO (Vehicle) and KO (CZP) are shown in (F). $n = 30$ (WT) and 30 (KO). Full statistical data are presented in Table S1.

[21, 23–25]. During NMDAR–dependent GABAergic iLTP, activated CaMKII phosphorylates target proteins such as gephyrin and the $GABA_AR$ β3 subunit to trigger *de novo* surface delivery of $GABA_ARs$ [21, 23–25, 37, 38, 49]. CaMKII-dependent phosphorylation at Ser^{305} of gephyrin regulates $GABA_AR$ diffusion and synaptic scaling at GABAergic postsynaptic sites [49, 58]. Similarly, phosphorylation of the $GABA_AR$ β3 subunit at Ser^{383} by CaMKII leads to reduced surface mobility and increased synaptic recruitment of $GABA_ARs$ [37, 38]. The present study has revealed that this activity-dependent upregulation of the surface $GABA_AR$ levels is carried out by the PX-RICS/GABARAP/14-3-3 trafficking complex (Supplementary Fig. 7). We have also identified PX-RICS as a downstream target of CaMKII. The phosphorylation–dependent interaction between PX-RICS and 14-3-3ζ/θ is thus a crucial regulatory point for GABAergic iLTP. Accumulating evidence has shown that other cell surface proteins depend on GABARAP for their surface expression [3]. Thus, the PX-RICS/GABARAP/14–3-3 trafficking complex may be widely implicated in the activity–dependent regulation of the membrane protein dynamics relevant to neural plasticity.

PX-RICS, GABARAP and 14-3-3ζ/θ are localized in the specific dendritic compartments that are immunopositive for organelle markers for the endoplasmic reticulum (ER), ER exit sites and the *trans*-Golgi network [3]. This structure, termed the dendritic satellite secretory pathway, is comprised of the dendritic ER and the Golgi outposts and is involved in the local synthesis, processing and transport of membrane-integral or secretory proteins in dendrites [59, 60]. The rapid increase in surface-expressed $GABA_ARs$ after NMDA stimulation could be explained by the localization of the PX-RICS–dependent trafficking machinery in the dendritic secretory compartments.

Several lines of evidence suggest that the dysregulation of GABA signaling underlies atypical social behavior in autism [3–18]. However, there has been no report describing deficits in GABAergic plasticity that contribute to autistic features. The present study has shown that PX-RICS is essential for GABAergic iLTP and that loss of the PX-RICS function in mice leads to impaired cued fear learning. Cued fear learning is closely associated with $GABA_AR$–mediated activity and plasticity in the amygdala [41, 42, 57] and is inversely correlated with the severity of autistic symptoms [54–56]. Considering all of these findings, we thus reason that PX-RICS–dependent $GABA_AR$ transport may play critical roles in emotional learning in the amygdala through the control of GABAergic synaptic plasticity and that the impairment of this transport mechanism may lead to improper socio-emotional processing, resulting in autistic-like atypical social behavior (Supplementary Fig. 7). Further

elucidation of the functional link between GABAergic plasticity and socio-emotional learning could lead to a better understanding of autism pathogenesis and treatment.

Funding Sources

This work was supported by JSPS KAKENHI Grant Number JP17K07104.

Declaration of Interests

The authors declare no conflict of interest.

Author Contributions

T.N. designed and performed all of the experiments except for the pain sensitivity test, analyzed the data and wrote the manuscript. F.S. performed fear conditioning and pain sensitivity tests and analyzed the data. Y.N.-N., Y.T. and K.M. bred mice and advised on animal experiments. T.A. supervised this study and wrote the manuscript.

Acknowledgments

The authors thank Dr. Stephen J. Moss for providing the anti-phospho-S^{383} antibody.

Appendix A. Supplementary data

Supplementary data to this article can be found online at https://doi.org/10.1016/j.ebiom.2018.07.011.

References

[1] Sztainberg Y, Zoghbi HY. Lessons learned from studying syndromic autism spectrum disorders. Nat Neurosci 2016;19(11):1408–17.
[2] Nelson SB, Valakh V. Excitatory/inhibitory balance and circuit homeostasis in autism spectrum disorders. Neuron 2015;87(4):684–98.
[3] Nakamura T, Arima-Yoshida F, Sakaue F, et al. PX-RICS-deficient mice mimic autism spectrum disorder in Jacobsen syndrome through impaired $GABA_A$ receptor trafficking. Nat Commun 2016;7:10861.
[4] Han S, Tai C, Westenbroek RE, et al. Autistic-like behaviour in $Scn1a^{+/-}$ mice and rescue by enhanced GABA-mediated neurotransmission. Nature 2012;489(7416):385–90.
[5] Penagarikano O, Abrahams BS, Herman EI, et al. Absence of CNTNAP2 leads to epilepsy, neuronal migration abnormalities, and core autism-related deficits. Cell 2011;147(1):235–46.
[6] Chao HT, Chen H, Samaco RC, et al. Dysfunction in GABA signalling mediates autism-like stereotypies and Rett syndrome phenotypes. Nature 2010;468(7321):263–9.
[7] Robertson CE, Ratai EM, Kanwisher N. Reduced GABAergic action in the autistic brain. Curr Biol 2016;26(1):80–5.
[8] Puts NA, Wodka EL, Harris AD, et al. Reduced GABA and altered somatosensory function in children with autism spectrum disorder. Autism Res 2017;10(4):608–19.
[9] Enticott PG, Kennedy HA, Rinehart NJ, Tonge BJ, Bradshaw JL, Fitzgerald PB. GABAergic activity in autism spectrum disorders: An investigation of cortical inhibition via transcranial magnetic stimulation. Neuropharmacology 2013;68:202–9.
[10] Oblak AL, Gibbs TT, Blatt GJ. Reduced $GABA_A$ receptors and benzodiazepine binding sites in the posterior cingulate cortex and fusiform gyrus in autism. Brain Res 2011;1380:218–28.
[11] Fatemi SH, Reutiman TJ, Folsom TD, Thuras PD. $GABA_A$ receptor downregulation in brains of subjects with autism. J Autism Dev Disord 2009;39(2):223–30.
[12] Chen CH, Huang CC, Cheng MC, et al. Genetic analysis of GABRB3 as a candidate gene of autism spectrum disorders. Mol Autism 2014;5:36.
[13] Piton A, Jouan L, Rochefort D, et al. Analysis of the effects of rare variants on splicing identifies alterations in $GABA_A$ receptor genes in autism spectrum disorder individuals. Eur J Hum Genet 2013;21(7):749–56.
[14] Delahanty RJ, Kang JQ, Brune CW, et al. Maternal transmission of a rare GABRB3 signal peptide variant is associated with autism. Mol Psychiatry 2011;16(1):86–96.
[15] Ma DQ, Whitehead PL, Menold MM, et al. Identification of significant association and gene-gene interaction of GABA receptor subunit genes in autism. Am J Hum Genet 2005;77(3):377–88.
[16] Sanders SJ, Ercan-Sencicek AG, Hus V, et al. Multiple recurrent de novo CNVs, including duplications of the 7q11.23 Williams syndrome region, are strongly associated with autism. Neuron 2011;70(5):863–85.
[17] Shao Y, Cuccaro ML, Hauser ER, et al. Fine mapping of autistic disorder to chromosome 15q11-q13 by use of phenotypic subtypes. Am J Hum Genet 2003;72(3):539–48.
[18] Warrier V, Baron-Cohen S, Chakrabarti B. Genetic variation in GABRB3 is associated with Asperger syndrome and multiple endophenotypes relevant to autism. Mol Autism 2013;4(1):48.
[19] Castillo PE, Chiu CQ, Carroll RC. Long-term plasticity at inhibitory synapses. Curr Opin Neurobiol 2011;21(2):328–38.
[20] Flores CE, Mendez P. Shaping inhibition: Activity dependent structural plasticity of GABAergic synapses. Front Cell Neurosci 2014;8:327.
[21] Mele M, Leal G, Duarte CB. Role of $GABA_AR$ trafficking in the plasticity of inhibitory synapses. J Neurochem 2016;139(6):997–1018.
[22] Petrini EM, Barberis A. Diffusion dynamics of synaptic molecules during inhibitory postsynaptic plasticity. Front Cell Neurosci 2014;8:300.
[23] Jacob TC, Moss SJ, Jurd R. $GABA_A$ receptor trafficking and its role in the dynamic modulation of neuronal inhibition. Nat Rev Neurosci 2008;9(5):331–43.
[24] Luscher B, Fuchs T, Kilpatrick CL. $GABA_A$ receptor trafficking-mediated plasticity of inhibitory synapses. Neuron 2011;70(3):385–409.
[25] Vithlani M, Terunuma M, Moss SJ. The dynamic modulation of $GABA_A$ receptor trafficking and its role in regulating the plasticity of inhibitory synapses. Physiol Rev 2011;91(3):1009–22.
[26] Marsden KC, Shemesh A, Bayer KU, Carroll RC. Selective translocation of Ca^{2+}/calmodulin protein kinase IIα (CaMKIIα) to inhibitory synapses. Proc Natl Acad Sci U S A 2010;107(47):20559–64.
[27] Marsden KC, Beattie JB, Friedenthal J, Carroll RC. NMDA receptor activation potentiates inhibitory transmission through GABA receptor-associated protein-dependent exocytosis of $GABA_A$ receptors. J Neurosci 2007;27(52):14326–37.
[28] Hayashi T, Okabe T, Nasu-Nishimura Y, et al. PX-RICS, a novel splicing variant of RICS, is a main isoform expressed during neural development. Genes Cells 2007;12(8):929–39.
[29] Okabe T, Nakamura T, Nishimura YN, et al. RICS, a novel GTPase-activating protein for Cdc42 and Rac1, is involved in the β-catenin-N-cadherin and N-methyl-D-aspartate receptor signaling. J Biol Chem 2003;278(11):9920–7.
[30] Nasu-Nishimura Y, Hayashi T, Ohishi T, et al. Role of the Rho GTPase-activating protein RICS in neurite outgrowth. Genes Cells 2006;11(6):607–14.
[31] Nakamura T, Hayashi T, Mimori-Kiyosue Y, et al. The PX-RICS-14-3-3ζ/θ complex couples N-cadherin-β-catenin with dynein-dynactin to mediate its export from the endoplasmic reticulum. J Biol Chem 2010;285(21):16145–54.
[32] Nakamura T, Hayashi T, Nasu-Nishimura Y, et al. PX-RICS mediates ER-to-Golgi transport of the N-cadherin/β-catenin complex. Genes Dev 2008;22(9):1244–56.
[33] De Rubeis S, He X, Goldberg AP, et al. Synaptic, transcriptional and chromatin genes disrupted in autism. Nature 2014;515(7526):209–15.
[34] Mezzavilla M, Ulivi S, Bianca ML, Carlino D, Gasparini P, Robino A. Analysis of functional variants reveals new candidate genes associated with alexithymia. Psychiatry Res 2015;227(2–3):363–5.
[35] Ohi K, Hashimoto R, Nakazawa T, et al. The p250GAP gene is associated with risk for schizophrenia and schizotypal personality traits. PLoS One 2012;7(4):e35696.
[36] Sumi M, Kiuchi K, Ishikawa T, et al. The newly synthesized selective Ca^{2+}/calmodulin dependent protein kinase II inhibitor KN-93 reduces dopamine contents in PC12h cells. Biochem Biophys Res Commun 1991;181(3):968–75.
[37] Petrini EM, Ravasenga T, Hausrat TJ, et al. Synaptic recruitment of gephyrin regulates surface $GABA_A$ receptor dynamics for the expression of inhibitory LTP. Nat Commun 2014;5:3921.
[38] Saliba RS, Kretschmannova K, Moss SJ. Activity-dependent phosphorylation of $GABA_A$ receptors regulates receptor insertion and tonic current. EMBO J 2012;31(13):2937–51.
[39] Bachman J. Site-directed mutagenesis. Methods Enzymol 2013;529:241–8.
[40] Carey MF, Peterson CL, Smale ST. PCR-mediated site-directed mutagenesis. Cold Spring Harb Protoc 2013;2013(8):738–42.
[41] Lange MD, Jungling K, Paulukat L, et al. Glutamic acid decarboxylase 65: A link between GABAergic synaptic plasticity in the lateral amygdala and conditioned fear generalization. Neuropsychopharmacology 2014;39(9):2211–20.
[42] Wiltgen BJ, Godsil BP, Peng Z, et al. The α1 subunit of the $GABA_A$ receptor modulates fear learning and plasticity in the lateral amygdala. Front Behav Neurosci 2009;3:37.
[43] Evans WO. A new technique for the investigation of some analgesic drugs on a reflexive behavior in the rat. Psychopharmacology (Berl) 1961;2:318–25.
[44] Swedberg MD. The mouse grid-shock analgesia test: pharmacological characterization of latency to vocalization threshold as an index of antinociception. J Pharmacol Exp Ther 1994;269(3):1021–8.
[45] Kamal A, Ramakers GM, Urban IJ, De Graan PN, Gispen WH. Chemical LTD in the CA1 field of the hippocampus from young and mature rats. Eur J Neurosci 1999;11(10):3512–6.
[46] Lee HK, Kameyama K, Huganir RL, Bear MF. NMDA induces long-term synaptic depression and dephosphorylation of the GluR1 subunit of AMPA receptors in hippocampus. Neuron 1998;21(5):1151–62.
[47] Snyder EM, Colledge M, Crozier RA, Chen WS, Scott JD, Bear MF. Role for A kinase-anchoring proteins (AKAPS) in glutamate receptor trafficking and long term synaptic depression. J Biol Chem 2005;280(17):16962–8.
[48] Rudolph U, Knoflach F. Beyond classical benzodiazepines: Novel therapeutic potential of $GABA_A$ receptor subtypes. Nat Rev Drug Discov 2011;10(9):685–97.
[49] Flores CE, Nikonenko I, Mendez P, Fritschy JM, Tyagarajan SK, Muller D. Activity-dependent inhibitory synapse remodeling through gephyrin phosphorylation. Proc Natl Acad Sci U S A 2015;112(1):E65–72.
[50] Ehrlich I, Humeau Y, Grenier F, Ciocchi S, Herry C, Luthi A. Amygdala inhibitory circuits and the control of fear memory. Neuron 2009;62(6):757–71.
[51] Johansen JP, Cain CK, Ostroff LE, LeDoux JE. Molecular mechanisms of fear learning and memory. Cell 2011;147(3):509–24.
[52] Baron-Cohen S, Ring HA, Bullmore ET, Wheelwright S, Ashwin C, Williams SC. The amygdala theory of autism. Neurosci Biobehav Rev 2000;24(3):355–64.

[53] Prager EM, Bergstrom HC, Wynn GH, Braga MF. The basolateral amygdala γ-aminobutyric acidergic system in health and disease. J Neurosci Res 2016;94(6):548–67.
[54] Banerjee A, Engineer CT, Sauls BL, Morales AA, Kilgard MP, Ploski JE. Abnormal emotional learning in a rat model of autism exposed to valproic acid in utero. Front Behav Neurosci 2014;8:387.
[55] Markram K, Rinaldi T, La Mendola D, Sandi C, Markram H. Abnormal fear conditioning and amygdala processing in an animal model of autism. Neuropsychopharmacology 2008;33(4):901–12.
[56] South M, Larson MJ, White SE, Dana J, Crowley MJ. Better fear conditioning is associated with reduced symptom severity in autism spectrum disorders. Autism Res 2011;4(6):412–21.
[57] Lu Y, Sun XD, Hou FQ, et al. Maintenance of GABAergic activity by neuregulin 1-ErbB4 in amygdala for fear memory. Neuron 2014;84(4):835–46.
[58] Battaglia S, Renner M, Russeau M, Come E, Tyagarajan SK, Levi S. Activity-dependent inhibitory synapse scaling is determined by gephyrin phosphorylation and subsequent regulation of $GABA_A$ receptor diffusion. eNeuro 2018;5(1) (ENEURO.0203-17.2017).
[59] Hanus C, Ehlers MD. Secretory outposts for the local processing of membrane cargo in neuronal dendrites. Traffic 2008;9(9):1437–45.
[60] Pierce JP, Mayer T, McCarthy JB. Evidence for a satellite secretory pathway in neuronal dendritic spines. Curr Biol 2001;11(5):351–5.